Raft-mediated trafficking of apical resident proteins occurs in both direct and transcytotic pathways in polarized hepatic cells

Slimane, TA; Trugnan, G; van Ijzendoorn, SCD; Hoekstra, D

Published in:
Molecular Biology of the Cell

DOI:
10.1091/mbc.E02-08-0528

Publication date:
2003

Molecular Biology of the Cell
Vol. 14, 611–624, February 2003

Raft-mediated Trafficking of Apical Resident Proteins Occurs in Both Direct and Transcytotic Pathways in Polarized Hepatic Cells: Role of Distinct Lipid Microdomains

Tounsia Aït Slimane,* Germain Trugnan,† Sven C.D. van IJzendoorn,* and Dick Hoekstra*‡

*Department of Membrane Cell Biology, University of Groningen, 9713 AV Groningen, The Netherlands; and †U538 Institut National de la Santé et de la Recherche Médicale, 75571 Paris, France

Submitted August 23, 2002; Revised October 4, 2002; Accepted October 25, 2002
Monitoring Editor: Suzanne R. Pfeffer

In polarized hepatic cells, pathways and molecular principles mediating the flow of resident apical bile canalicular proteins have not yet been resolved. Herein, we have investigated apical trafficking of a glycosylphosphatidylinositol-linked and two single transmembrane domain proteins on the one hand, and two polytopic proteins on the other in polarized HepG2 cells. We demonstrate that the former arrive at the bile canalicular membrane via the indirect transcytotic pathway, whereas the polytopic proteins reach the apical membrane directly, after Golgi exit. Most importantly, cholesterol-based lipid microdomains ("rafts") are operating in either pathway, and protein sorting into such domains occurs in the biosynthetic pathway, largely in the Golgi. Interestingly, rafts involved in the direct pathway are Lubrol WX insoluble but Triton X-100 soluble, whereas rafts in the indirect pathway are both Lubrol WX and Triton X-100 insoluble. Moreover, whereas cholesterol depletion alters raft-detergent insolubility in the indirect pathway without affecting apical sorting, protein missorting occurs in the direct pathway without affecting raft insolubility. The data implicate cholesterol as a traffic direction-determining parameter in the direct apical pathway. Furthermore, raft-cargo likely distinguishing single vs. multispanning membrane anchors, rather than rafts per se (co)determine the sorting pathway.

INTRODUCTION

Polarized cells display two structurally and functionally different plasma membrane domains, i.e., the apical and basolateral domain, separated by tight junctions. The generation of the distinct molecular identity of both domains and its maintenance in spite of the dynamics of lipids and proteins at either surface requires sophisticated sorting and trafficking mechanisms. Indeed, many proteins, transported along the secretory pathway, contain specific sorting signals, such as those based on Tyr- and diLeu-based amino acid motifs, which are recognized by distinct molecular subunits of adaptor complexes, a pivotal mechanism in basolateral targeting (Matter and Mellman, 1994). Liquid-ordered sphingolipid/cholesterol-enriched domains, also known as "rafts," seem instrumental in targeting of apical proteins (Simons and Ikonen, 1997; Ikonen, 2001). Sorting signals are provided by their glycosylphosphatidylinositol (GPI)-membrane anchor (Brown *et al.*, 1989; Lisanti *et al.*, 1989, 1990) or transmembrane domain (TMD) (Kundu *et al.*, 1996; Huang *et al.*, 1997; Lin *et al.*, 1998). These sorting principles in polarized trafficking have been largely derived in Madin-Darby canine kidney (MDCK) cells. In these cells, a so-called "direct" sorting pathway operates in that newly synthesized proteins are primarily sorted in the *trans*-Golgi Network (TGN) and directly delivered to the apical or basolateral membrane (Rodriguez-Boulan and Powell, 1992). However, depending on polarized cell type, it has been shown that resident apical proteins may also be sorted in an "indirect" or transcytotic pathway. In this case, they are first sent from the TGN to the basolateral surface, from where they are endocytosed and subsequently transported to the opposite, apical surface (for review, see Mostov *et al.*, 2000; Nelson and Yeaman, 2001).

It is unknown why polarized cells exploit to different extents both these pathways for generating cell polarity. Nevertheless, hepatocytes seem to represent an extreme case

Article published online ahead of print. Mol. Biol. Cell 10.1091/mbc.E02–08–0528. Article and publication date are at www.molbiolcell.org/cgi/doi/10.1091/mbc.E02–08–0528.

‡ Corresponding author. E-mail address: d.hoekstra@med.rug.nl

in that it has been suggested that these polarized cells lack a direct route for the apical delivery of proteins all together, and predominantly use the indirect pathway (Bartles *et al.*, 1987; Schell *et al.*, 1992; Maurice *et al.*, 1994; Ihrke *et al.*, 1998). Yet, evidence has been presented that in HepG2 cells, a well-polarized human hepatoma cells, newly synthesized sphingolipids can reach the apical bile canalicular (BC) membrane directly, without a need for prior delivery to the basolateral membrane (Zegers and Hoekstra, 1997). This would suggest that a direct vesicular transport pathway between TGN and BC membrane does exist in hepatocytes, raising the question whether and if so which proteins might participate in this transport event. Very recently, such a direct pathway for the polytopic apical plasma membrane ATP-binding cassette (ABC) transporter proteins, multidrug resistance protein 1 (MDR1), and sister of p-glycoprotein (SPGP) has been proposed, based upon in vitro and in vivo experiments in liver cells (Sai *et al.*, 1999; Kipp and Arias, 2000). Most importantly, these data question the long-standing dogma of an exclusive indirect transfer of resident apical proteins in liver cells.

Herein, we addressed the questions 1) whether a direct pathway for protein transport also exists in polarized HepG2 cells, and if so, which structural parameters of the protein govern its entry in either pathway; and 2) given the dynamics of sphingolipid trafficking in both basolateral and apical direction as well as along the transcytotic pathway (van IJzendoorn and Hoekstra, 1999a; Maier *et al.*, 2001), whether and when a raft mechanism comes into play in apical (AP) sorting and trafficking of proteins in these cells.

Our data reveal, for the first time, that distinct lipid microdomains, as characterized by differences in detergent insolubility, are operating in both direct and indirect apical transport of resident AP proteins in liver cells. Direct sorting is at least partly dependent on the presence of raft-localized cholesterol, a pathway that seems to be preferred by polytopic membrane proteins.

MATERIALS AND METHODS

Reagents

Media and reagents for cell culture were purchased from Invitrogen (Carlsbad, CA). [^{35}S]Methionine/cysteine "in vitro cell lab mix," nitrocellulose, and the enhanced chemiluminescence kit were from Amersham Biosciences (Piscataway, NJ). Protein A-Sepharose was from Pharmacia AB (Uppsala, Sweden). LubWX (Lubrol 17A17) was from Serva (Heidelberg, Germany). BODIPY-sphingomyelin (SM) was from Molecular Probes (Eugene, OR). Fluorescent secondary antibodies were from Jackson Immunoresearch Laboratories West Grove, PA). All other reagents were obtained from Sigma-Aldrich (St. Louis, MO).

Primary Antibodies

Monoclonal antibodies (mAbs) (C219 and 4E3) directed against MDR1 were from Signet Laboratories (Dedham, MA). A mAb anti-caveolin-1 (cav-1) was purchased from Transduction Laboratories (Lexington, KY). A polyclonal antibody (pAb) anti-actin was from Santa Cruz Biotechnology (Santa Cruz, CA). A pAb against aminopeptidase N (APN) was provided by Dr. Ann. Hubbard (Johns Hopkins University School of Medicine, Baltimore, MD). mAbs directed against human ATP7B and human dipeptidylpeptidase IV (DPPIV) (HBB3/775) were provided by Dr. Han Roelofsen (Department of Paediatrics, University of Groningen, Groningen, The Netherlands) and Dr. Hans-Peter Hauri (Biozentrum der Universität Basel, Basel, Switzerland), respectively. A pAb against green fluorescent protein (GFP) was provided by Jean-Louis Delaunay (Institut National de la Santé et de la Recherche Médicale, CHU St-Antoine, Paris, France).

Cell Culture

HepG2 and MDCK cells were grown at 37°C in DMEM supplemented with 10% heat-inactivated (56°C, 30 min) fetal bovine serum, 2 mM L-glutamine, 100 U/ml penicillin, and 100 μg/ml streptomycin, under a 5% CO_2, air atmosphere. For microscopy and biochemistry experiments, HepG2 cells were grown onto glass coverslips and 60-mm dishes, respectively. To allow access to either the AP or basolateral (BL) membranes of MDCK monolayers, cells were grown on tissue culture-treated polycarbonate Transwell filters.

Constructs, Transfection, and Clonal Selection

HepG2 cells were transfected with cDNAs encoding MDR1-GFP, GPI-GFP, and cav-1 constructs. The MDR1-GFP construct, prepared as described in Sai *et al.* (1999), was a kind gift of Dr. Irwin M. Arias (Tufts University School of Medicine, Boston, MA). GPI-GFP and cav-1 constructs were from Andre Le Bivic (IBDM Faculte des Sciences de Luminy, Marseille, France). GPI-GFP was produced by fusion of the human decay accelerating factor GPI-anchoring sequence with GFP. Canine cav-1 was cloned in the PCDNA3 plasmid. Cells were transfected with the cationic lipid SAINT-2, according to a procedure previously described by van der Woude *et al.* (1997). Briefly, cells were seeded in 35-mm dishes at low density, and the transfection was performed the following day. To this end, small unilamellar vesicles, consisting of SAINT-2/dioleoylphsophatidylethanolamine, molar ratio 1:1, were prepared by sonication. These vesicles (15 μl; 1 mM stock solution) were mixed with 1 μg of plasmid DNA. Cells were transfected for 6 h. After 48 h, selection was started by addition of G418. Stable clones were isolated using cloning cylinders. Cells were screened by direct GFP fluorescence.

Indirect Immunofluorescence and Confocal Microscopy

Cells were washed with phosphate-buffered saline $(PBS)^+$ (0.5 mM $CaCl_2$ and 1 mM $MgCl_2$), fixed with 4% paraformaldehyde for 1 min at 4°C, and permeabilized in methanol for 10 min at 4°C. After blocking in 1% PBS/bovie serum albumin (BSA), cells were incubated for 1 h at room temperature with primary antibodies. After three washes in PBS, cells were incubated for 1 h at room temperature with fluorescently labeled secondary antibodies. After three washes in PBS, cells were incubated for 10 min with RNAse A and then for 1 min with propidium iodide to stain nuclei. For detergent extraction on living cells, the cells were put on ice, washed three times with PBS^+, and incubated for 5 min in 1% detergent/PIPES buffer (80 mM PIPES, pH 6.8, 5 mM EGTA, 1 mM $MgCl_2$). The buffer was removed, and cells were fixed and processed as for immunofluorescence. Fluorescence was examined by confocal microscopy (TCS SP2; Leica, Wetzlar, Germany). Optical sections were recorded with a 63/1.4 immersion objective. Laser scanning confocal images were collected and analyzed using the on-line ScanWare software. Images were processed using Adobe software.

Transcytosis Assay

Transcytosis assays for protein trafficking were performed according to previously published protocol (Ihrke *et al.*, 1998). Briefly, after three washes with HEPES-buffered serum-free medium (HSFM), stably transfected HepG2 cells were incubated for 30 min on ice with primary antibodies diluted in HSFM/0.2% BSA. After surface labeling, cells were extensively washed with HSFM/0.2% BSA and

chased in normal medium at 37°C for various periods of time. After the chase, cells were washed, fixed with paraformaldehyde/methanol, blocked 1 h with PBS/1% BSA, and incubated with fluorescently labeled secondary antibodies. Fluorescence was examined by confocal scanning microscopy.

Detergent-resistant Membrane (DRM) Preparation and Analysis

Cells grown to confluence were rinsed with PBS and lysed for 20 min in TNE (20 mM Tris-HCl pH 7.4, 150 mM NaCl, 1 mM EDTA, 1% Triton X [TX] 100 or 1% LubWX, and protease inhibitors) buffer on ice. Lysates were scraped from the dishes and homogenized by passing through a 22-gauge needle. The extracts were brought to 40% sucrose and placed at the bottom of 5–35% sucrose gradient. Gradients were centrifuged for 20 h at 38,000 rpm at 4°C in a Beckman SW 41 rotor. Fractions of 1 ml were harvested from the top of the gradient. Proteins were recovered by trichloroacetic acid (TCA) precipitation. The TCA pellets were solubilized in Laemmli buffer before running the samples on SDS-PAGE. After transfer to nitrocellulose, proteins were detected with specific antibodies, and revealed by enhanced chemiluminescence kit.

Metabolic Labeling, Detergent Extraction, and Immunoprecipitation

Cells were first incubated for 2 × 30 min at 37°C in methionine/cysteine-free medium, and pulse labeled with 300 μCi/ml of [^{35}S]methionine/cysteine at 37°C. After a wash with DMEM, cells were chased at 37°C in DMEM containing excess cysteine and methionine (2 and 1 mM, respectively) for the indicated periods. After each time point, cells were washed with PBS^{+} on ice and lysed for 20 min on ice in 1 ml of TNE/TX-100 or TNE/LubWX buffer. Lysates were collected and centrifuged at 13,000 rpm for 2 min at 4°C. Supernatants, representing the soluble material, were separated from pellets that were solubilized in 100 μl of solubilization buffer (50 mM Tris-HCl pH 8.8, 5 mM EDTA, 1% SDS). Both soluble and insoluble fractions were adjusted to 0.1% SDS and then immunoprecipitated at 4°C. After washing, immunoprecipitates were analyzed by SDS-PAGE. Gels were dried and submitted to fluorography. The fluorograms were scanned and the bands were quantified using Scion Image software.

Miscellaneous Procedures

Cholesterol Depletion of HepG2 Cells. Lovastatin and methyl-β-cyclodextrin (Lov/CD) treatment was carried out as described previously (Keller and Simons, 1998) with some modifications adapted to HepG2 cells. Briefly, HepG2 cells were plated on 60-mm dishes, lovastatin (8 μM) was added 24 h after plating, and the cells were subsequently allowed to grow for another 48 h. The cells were then incubated for 30 min under agitation with 10 mM CD diluted in serum-free medium containing 10 mM HEPES pH 7.5.

Cholesterol Replenishment of HepG2 Cells. Replenishment of depleted cholesterol was carried out by incubating the cells with preformed cyclodextrin/cholesterol complexes as described previously (Zuhorn *et al.*, 2002). Briefly, after cholesterol depletion, HepG2 cells were washed with serum-free medium and incubated 3 h at 37°C in the presence of CD-cholesterol (CD/Chol) complexes (400 μg/ml cholesterol) diluted in serum-free medium and subsequently used for cholesterol determination or for MDR1-GFP distribution.

Cholesterol Determination. The cholesterol concentration in control, cholesterol-depleted, and cholesterol-repleted cells was determined spectrophotometrically by a cholesterol oxidase/peroxidase assay (Gamble *et al.*, 1978).

RESULTS

GPI-GFP Traffics Along the Indirect Route to the AP Surface of HepG2 Cells

As a model for a known lipid raft-associated GPI-anchored protein (Nichols *et al.*, 2001), a class of proteins typically targeted to the apical membrane of common epithelial cells (Brown *et al.*, 1989; Lisanti *et al.*, 1989, Garcia *et al.*, 1993; Kenworthy and Edidin, 1998), we first examined the steady-state distribution of the GPI-GFP fusion protein in polarized HepG2 cells. As shown in Figure 1A, a, in stably transfected cells, green fluorescence was prominently present at the BC membrane, whereas a fraction of the protein was also discerned at the BL surface. Staining of GPI-GFP–expressing cells with anti-GFP antibody confirmed this distribution (Figure 1A, b).

As a negative control, cells were also transfected with GFP alone. In this case, fluorescence was distributed randomly throughout the cell (our unpublished data), thus excluding a GFP-mediated effect on the distribution of the GPI-GFP fusion protein (cf. Zacharias *et al.*, 2002).

It has been proposed that polarized hepatic cells transport most of their resident AP proteins first to the BL surface, where they are internalized and redirected to the AP surface by transcytosis (Schell *et al.*, 1992; Hemery *et al.*, 1996; Ihrke *et al.*, 1998; Bastaki *et al.*, 2002).

To determine whether GPI-GFP uses the transcytotic pathway in HepG2 cells, we performed an antibody-trafficking assay (Ihrke *et al.*, 1998). In addition, to investigate whether and how the nature of membrane anchorage may affect the transcytotic processing of resident AP proteins, we analyzed in parallel the trafficking behavior of endogenous DPPIV, an AP resident single TMD protein that has been extensively used as a model protein to study sorting mechanisms in a variety of epithelia. When transfected in MDCK cells, DPPIV is targeted directly from the TGN to the apical domain (Casanova *et al.*, 1991; Low *et al.*, 1991), whereas in intestinal cells, endogenous DPPIV is partly directly transported to the apical membrane, whereas the remainder travels apically via the basolateral domain (Le Bivic *et al.*, 1990; Matter *et al.*, 1990). In Fisher rat thyroid cells, DPPIV sorting depends on the onset of cell differentiation, i.e., transcytosis decreases and direct apical targeting increases in more differentiated cells (Zurzolo *et al.*, 1992). GPI-GFP–expressing cells were incubated for 30 min at 0°C with antibodies to GFP or DPPIV to allow their binding to the surface of HepG2 cells. Trafficking was initiated by raising the temperature to 37°C. After various chase periods, the cells were fixed, permeabilized and incubated with fluorescently labeled secondary antibodies. As shown in Figure 1B, a and a′, after an incubation on ice, anti-GFP and anti-DPPIV were exclusively localized at the BL membrane, implying that the tight junctions effectively precluded access of antibodies to the AP surface. At 37°C, both GPI-GFP and DPPIV became internalized as a function of time, as reflected by a decrease in basolateral and a concomitant increase in intracellular staining (Figure 1B, b, c, b′, and c′). After 180 min, a prominent and homogeneous distribution of both antibody-conjugated proteins at the BC surface was apparent (Figure 1B, d and d′). These results thus indicate that resident AP membrane proteins may reach the BC membrane in HepG2 cells along an indirect, transcytotic pathway. Interestingly, transcytotic transport of DPPIV seemed considerably more efficient than that of the GPI-GFP over this

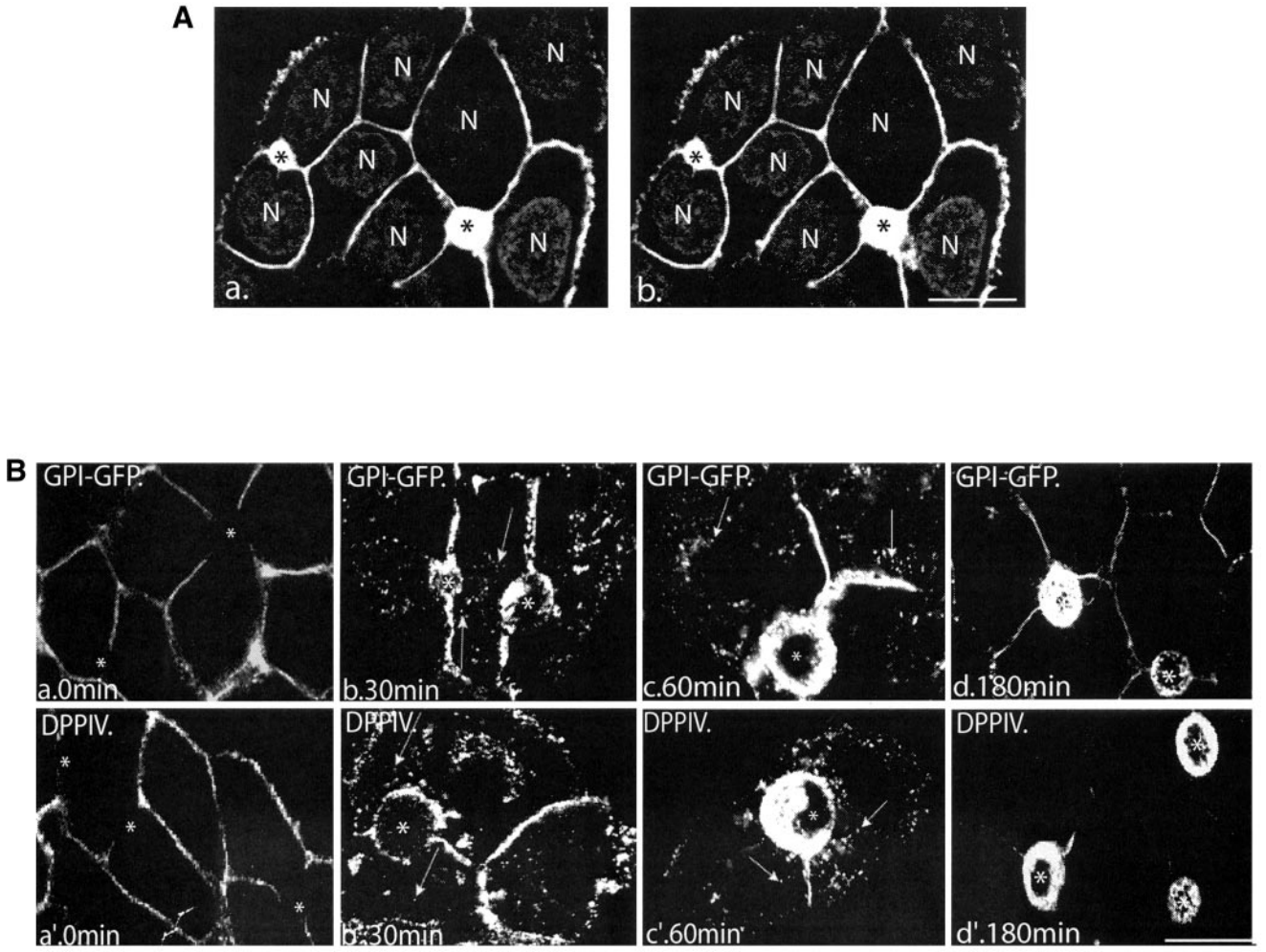

Figure 1. GPI-GFP is localized at the BC membrane of HepG2 cells, reached by the indirect pathway. (A) GPI-GFP–transfected cells were grown on coverslips, fixed, permeabilized, and stained with the anti-GFP antibody and secondary Cy5-conjugated antibody. Confocal microscopy shows that at steady state the GFP fluorescence preferentially localizes at the BC surface (a, asterisk), but is also detected at the BL membrane. Staining with anti-GFP antibody confirms this distribution (b). Nuclei (N) are stained with propidium iodide. (B) BL-to-AP transcytosis of GPI-GFP and DPPIV was monitored by an antibody-immunoassay. GPI-GFP–expressing cells were incubated for 30 min at 0°C with anti-GFP (a–d) or anti-DPPIV antibodies (a′–d′). Immediately (a and a′) or after 30 (b and b′), 60 (c and c′), or 180 min (d and d′) at 37°C, cells were fixed and permeabilized. Primary antibodies were visualized with secondary TRITC-(GFP)– or Cy3-(DPPIV)–conjugated antibodies. For each time point, a minimum of 50 BC structures was analyzed in three independent experiments. BCs are marked by asterisks; arrows (b, c, b′, and c′) point to GPI-GFP– and DPPIV-positive vesicles detected during internalization of both antibody-conjugated proteins. Bar, 10 μm.

time period (Figure 1B, d vs. d′). Obviously, a number of mechanisms could underlie this difference, including differences in sorting and/or transport efficiency. Both these events might be related to the nature of membrane microdomains in which either protein could partition. Thus far, the presence of such domains in liver cells has neither been revealed nor investigated.

GPI-GFP and DPPIV Are Incorporated into TX-100–insoluble Microdomains with Different Efficiencies

To address the question whether a raft transport mechanism is at all operational in liver cells, we extracted a cell lysate of GPI-GFP–transfected cells with TX-100 in the cold, which was then centrifuged to equilibrium on a sucrose density gradient. In comparison with cav-1, an established marker for DRM fractions, also GPI-GFP was highly enriched in the lighter fractions of the gradient, whereas negligible amounts were localized in the heavier, soluble fractions (Figure 2A). Accordingly, these data imply that the GPI-linked protein is almost exclusively integrated into TX-100–insoluble microdomains in HepG2 cells. In case of DPPIV, only a minor fraction was found to be associated with TX-100-insoluble microdomains, the major fraction being detergent soluble (Figure 2A).

These results demonstrate that lipid microdomains are present in polarized hepatic cells and that at steady state

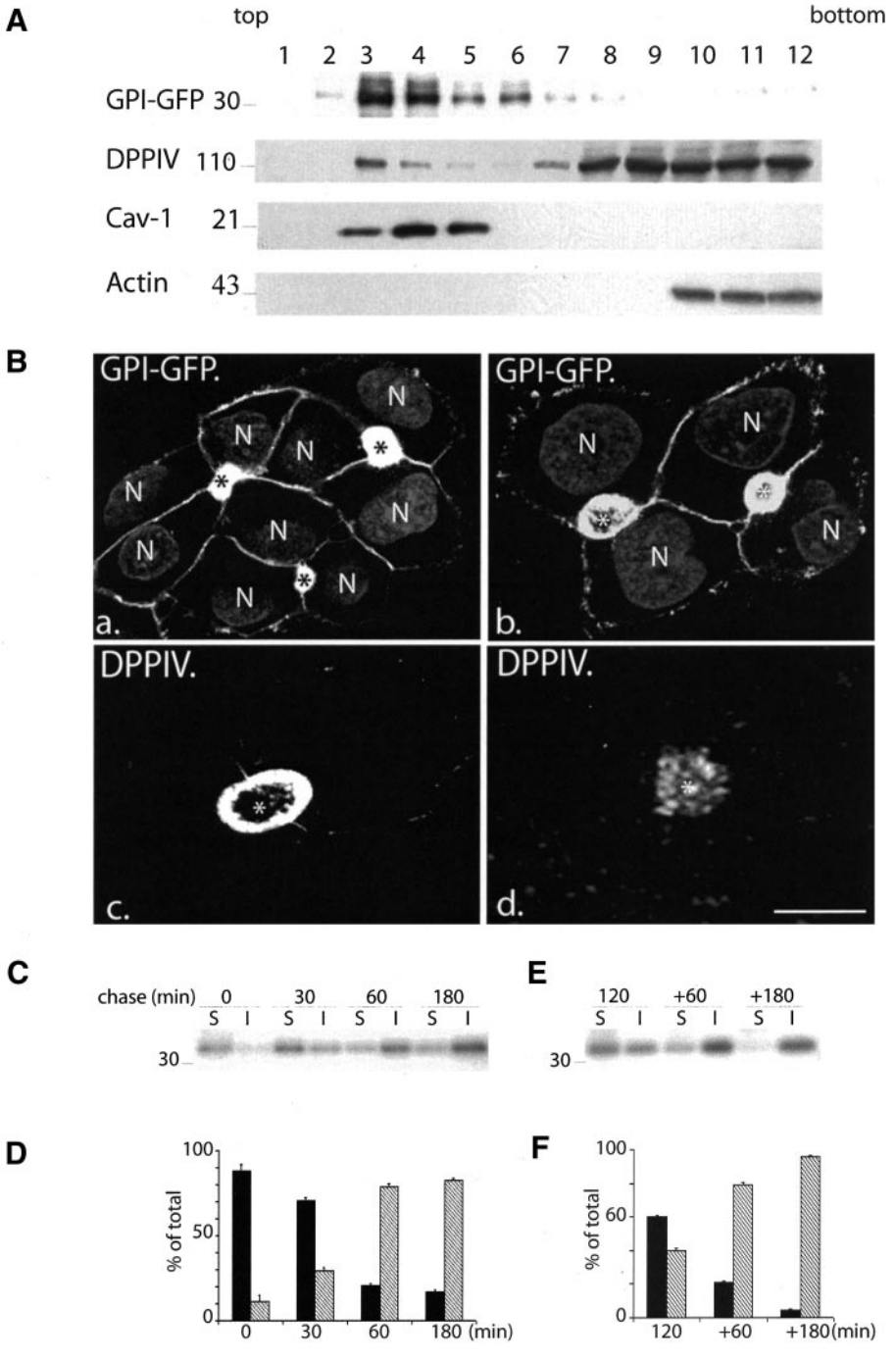

Figure 2. GPI-GFP and DPPIV are recruited in TX-100–insoluble microdomains. (A) GPI-GFP–expressing cells were lysed in TNE/TX-100 buffer at 4°C and run through a 5–40% sucrose gradient. For DPPIV analysis, HepG2 cells were ^{35}S-labeled for 6 h, and after lysis fractionated on a similar gradient. Cav-1, stably expressed in HepG2 cells, was analyzed in parallel as a marker to indicate DRM fractions. Actin was used as a negative control. Fractions of 1 ml were collected from top to bottom after centrifugation to equilibrium. GPI-GFP, Cav-1, and actin were TCA precipitated, whereas labeled DPPIV was immunoprecipitated. (B) GPI-GFP–expressing cells were fixed and analyzed for the presence of GPI-GFP and DPPIV either directly (a and c) or after in situ extraction with 1% TX-100 (b and d). *, BC. Bar, 10 μm. (C) GPI-GFP–expressing cells were pulse chased with [^{35}S]methionine for 10 min, followed by incubation in chase medium for the indicated times. After extraction in TNE/TX-100 buffer at 4°C, both the soluble (S; supernatant) and insoluble (I; pellet) fractions were collected by centrifugation, immunoprecipitated, and analyzed by SDS-PAGE. Quantification of three independent experiments is shown in D as mean ± SD. Black bars represent soluble protein and hatched bars represent insoluble protein. (E) Pulse chase analysis of GPI-GFP after a temperature block. After a short pulse (10 min), GPI-GFP–expressing cells were chased for 120 min at 20°C and then warmed to 37°C and chased for another 60 and 180 min. Quantification of three independent experiments is shown in F as mean ± SD. Black bars represent soluble protein and hatched bars represent insoluble protein.

both the GPI-anchored and single TMD protein associate with TX-100–insoluble microdomains. Yet, quantitatively, their partitioning into such domains differed dramatically, a feature that could explain the observed differences in their kinetics of processing (Figure 1B), and/or suggest differences in lateral distribution (see below). Most intriguingly, because at steady-state conditions almost the entire fraction of GPI-GFP was recovered from TX-100–insoluble domains, the data could imply that the AP protein fraction present near or at the BL membrane is also localized in lipid microdomains. Indeed, in situ extraction revealed that whereas only a minor fraction of DPPIV resists TX-100 extraction, GPI-GFP remained firmly associated with both the BC and the BL surface (Figure 2B). This result is entirely compatible with the notion that transcytotic transport and sorting of GPI-GFP relies on its integration into DRM, directed to and

present at both the AP and BL membrane domains of HepG2 cells. Apparently, the efficiency of overall exploitation of this mechanism for indirect transport of AP resident protein in liver cells depends on the nature of the protein, as suggested by the lower partitioning of DPPIV in such domains (but see below; Figure 7B).

GPI-GFP Is Incorporated into TX-100–insoluble Domains in the Biosynthetic Pathway

To determine where DRM association of GPI-GFP potentially occurred, detergent resistance was determined in a pulse/chase experiment. As shown in Figure 2, C and D, after a 15-min pulse, GPI-GFP was almost totally soluble. After 30-min chase, a shift was seen from the TX-100–soluble to the TX-100–insoluble fractions, whereas between 30 and 60 min, the major GPI-GFP fraction (80%) had become detergent resistant, which increased to almost complete resistance over the next 180 min. In light of the kinetics of surface membrane transport of newly synthesized membrane proteins, the data suggest that the GPI-linked GFP became integrated into lipid microdomains well before reaching the surface of HepG2 cells. Indeed, when pulsed cells were chased for 2 h at 20°C to accumulate newly synthesized GPI-GFP in the Golgi complex, ~40% of the protein was recovered in the insoluble fraction. After an additional chase at 37°C, i.e., when trafficking resumed at optimal conditions, the protein became almost totally insoluble (Figure 2, E and F). These results indicate that GPI-GFP–containing DRM were, at least in part, assembled at the level of the Golgi.

MDR1-GFP Is Detected Exclusively at the BC Membrane of HepG2 Cells

The data are in line with the existence of a raft-mediated indirect, transcytotic pathway for AP resident proteins in polarized hepatic cells, a prerogative thus far thought to be exclusively associated with direct AP transport. We therefore investigated in the present system in a direct manner the principle of sorting and transport of the ABC transporter MDR1, which has been claimed to travel along the direct pathway from the TGN to the BC membrane in hepatic cells (Sai *et al.*, 1999; Kipp and Arias, 2000). To verify that the MDR1-GFP protein was biosynthetically processed like its natural counterpart, its posttranslational processing was examined in a pulse/chase experiment. As shown in Figure 3A, newly synthesized MDR1-GFP showed as a doublet corresponding to the high mannose (h) and the complex (c) forms. After 60 min, the fusion protein was exclusively present as a mature (complex) glycoprotein. The steady-state distribution of the protein was subsequently revealed by direct visualization of GFP fluorescence, and by antibody probing, directed against GFP or MDR1. As shown in Figure 3, B and C, the protein was exclusively associated with the BC membrane, i.e., MDR1-GFP could not be detected at the BL membrane of HepG2 cells. Finally, the described localization of the fusion protein is entirely in line with that of endogenous MDR1, when visualized (in nontransfected cells) after staining with the MDR1-antibody (our unpublished data). Accordingly, these data exclude that the attachment of GFP could have affected the localization and processing of MDR1 (cf. Zacharias *et al.*, 2002).

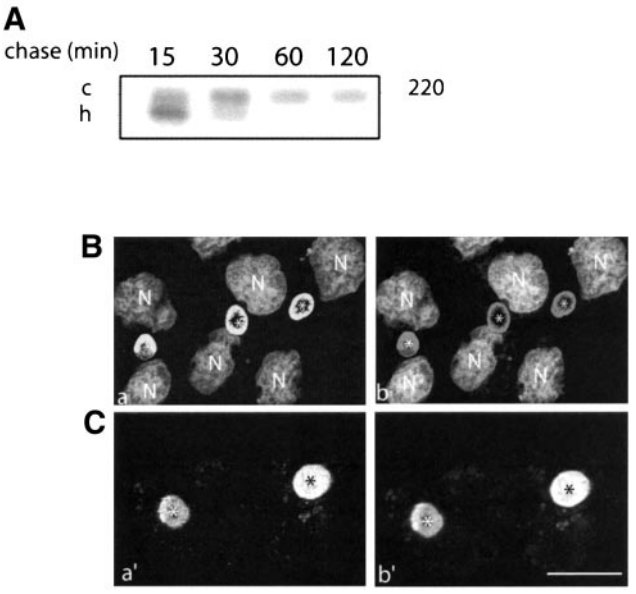

Figure 3. MDR1-GFP is localized at the BC surface of HepG2 cells. (A) MDR1-GFP–transfected cells were biosynthetically labeled for 10 min with [^{35}S]methionine and chased for the indicated times. Samples were immunoprecipitated with pAb against GFP and analyzed on SDS-PAGE. In B and C, transfected HepG2 cells were directly visualized for GFP fluorescence localization (a and a′), or examined after staining with either anti-GFP (B, b) or anti-MDR1 (C, b′). Nuclei (N) stained with propidium iodide. *, BC. Bar, 10 μm.

To obtain further support for a direct pathway for MDR1 transport in HepG2 cells, the trafficking antibody assay was carried out as described above, by using the specific mAb 4E3, which reacts with an external epitope of MDR1 (Gribar *et al.*, 2000). Because the HepG2 cell system precludes direct access to the BC, appropriate recognition of the external epitope on the GFP-MDR1 construct was first examined in polarized MDR1-GFP–expressing MDCK cells. GFP fluorescence was restricted to the AP surface (Figure 4A, a) and consistent with this localization, when mAb 4E3 was added to the AP and BL surface of nonpermeabilized and fixed filter-grown MDCK cells, anti-4E3 staining was similarly exclusively detected at the AP surface (Figure 4A, b). We conclude therefore that the external epitope of MDR1 is recognized by the mAb. In live HepG2 cells we then monitored the dynamics of MDR1-GFP, and in parallel, that of another apical resident protein, the single TMD protein APN. MDR1-GFP–expressing cells were incubated for 30 min at 0°C with antibodies to MDR1 or APN and then fixed and stained with fluorescently labeled secondary antibodies. Neither under these conditions nor after an overnight incubation at 37°C with the mAb 4E3 could any staining be detected (Figure 4B, a), thus strongly suggesting that MDR1 never reached the BL membrane of HepG2 cells. In contrast, after the 0°C incubation, APN displayed a strong labeling at the BL surface (Figure 4B, b). After 30 min at 37°C, its vesicular transport was readily revealed by the extensive punctate intracellular fluorescence (Figure 4B, c). After 180 min, the predominant presence of the protein at the BC

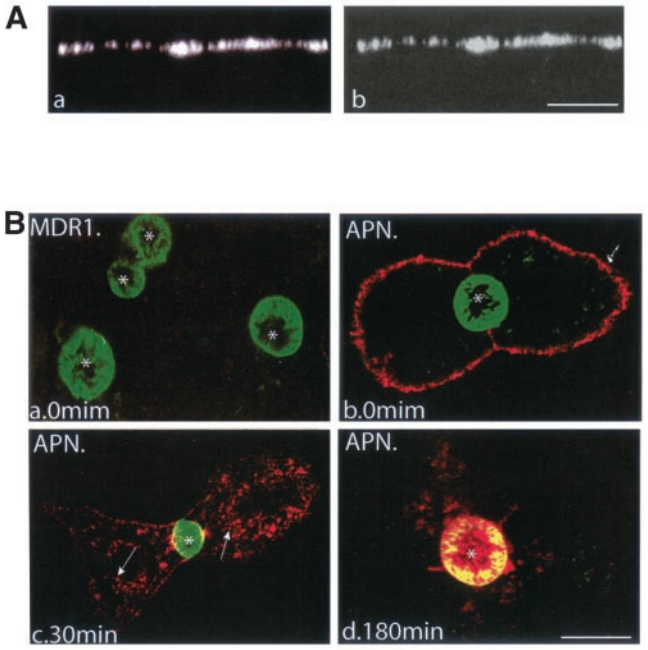

Figure 4. Direct transport of MDR1-GFP in HepG2 cells as detected by mAb 4E3. (A) MDCK cells stably transfected with MDR1-GFP were grown on Transwell filters, fixed, and visualized directly (a) or after staining with mAb 4E3 added to both the AP and BL sides (b). The XZ sections show that MDR1-GFP is restricted to the AP surface of MDCK cells. (B) BL-to-AP-transcytosis of MDR1-GFP and APN in HepG2 cells. MDR1-GFP–expressing cells were incubated for 30 min at 0°C with mAb 4E3 (a) or anti-APN antibody (b–d). After washing, cells were either fixed and permeabilized immediately (a and b) or warmed to 37°C for 30 min (c) and 180 min (d), and stained with secondary Cy3- (MDR1) or TRITC-(APN)-conjugated antibodies. *, BC, arrows (c) point to APN-positive vesicles detected during internalization of the antibody-conjugated complex. Bar, 10 μm.

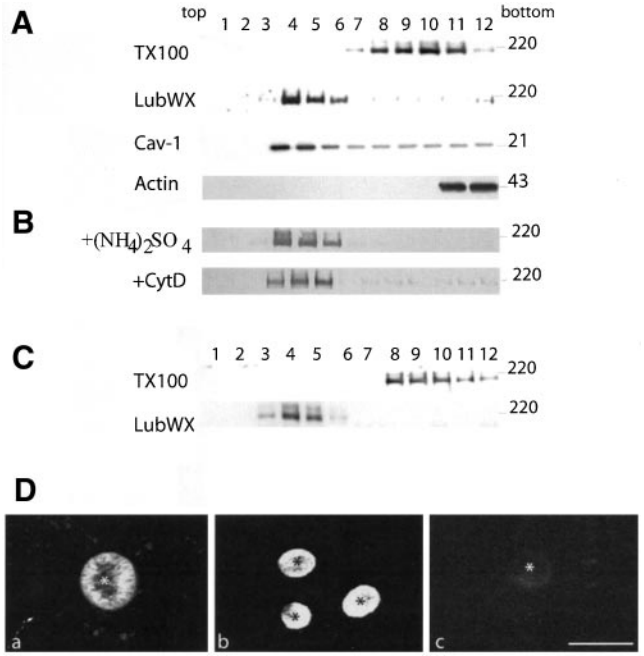

Figure 5. MDR1-GFP localizes to LubWX-insoluble microdomains and is solubilized in TX-100. (A) MDR1-GFP–expressing HepG2 cells were lysed either in TNE/TX-100 buffer or TNE/LubWX buffer at 4°C and analyzed by flotation on sucrose gradient. For details, see legend to Figure 2. Cav-1 and actin were analyzed in parallel as positive and negative controls, respectively. (B) Insolubility of MDR1-GFP in LubWX is not due to interaction with cytoskeletal elements. MDR1-GFP–expressing cells were lysed in 1% LubWX at 4°C in the presence of 250 mM $(NH_4)_2SO_4$ [(+$NH_4)_2SO_4$] or incubated for 1 h at 37°C in the presence of 10 μg/ml cytochalasin D (+CytD) followed by lysis in 1% LubWX at 4°C. (C) A similar analysis as in A was carried out in MDR1-GFP–transfected MDCK cells. (D) Analysis of MDR1-GFP association with lipid microdomains after in situ extraction with detergents. MDR1-GFP–expressing cells were either fixed directly (a) or extracted with 1% LubWX (b) or 1% TX 100 (c) before fixation.

membrane was apparent, as indicated by its colocalization with the (green) fluorescence of MDR1-GFP (Figure 4B, d). Accordingly, these results clearly distinguish the transcytotic pathway taken by APN (or GPI-GFP and DPPIV; see above) to the BC membrane from the direct pathway, taken by MDR1-GFP.

MDR1-GFP Is Soluble in TX 100 but Insoluble in LubWX

Are lipid microdomains also involved in the direct transport pathway, marked by MDR1-GFP, in polarized HepG2 cells? On solubilization in TX-100, MDR1-GFP was not found to float to the light fractions, corresponding to DRM (Figure 5A), indicating that at steady state MDR1-GFP was not associated with TX-100–insoluble microdomains. Rather, when the cells were extracted with 1% LubWX, MDR1-GFP was found to float to the low-density fractions (Figure 5A). To rule out the possibility that insolubility of MDR1-GFP in LubWX was due to its interaction with cytoskeletal elements, MDR1-GFP–expressing cells were lysed using a buffer containing 250 mM $(NH_4)_2SO_4$ to disrupt the cytoskeleton (Roper *et al.*, 2000) or treated with the actin-disrupting drug cytochalasin D before LubWX extraction. As shown in Figure 5B, at either condition, the proportion of MDR1-GFP recovered in the low-density fractions was the same as in nontreated cells, thus excluding artifacts due to interaction with cytoskeletal elements.

To examine whether MDR1-GFP localization in LubWX-insoluble microdomains was specific for HepG2 cells, we analyzed in parallel the DRM-association of MDR1-GFP in MDCK cells. As shown in Figure 5C, like in HepG2 cells, MDR1-GFP floated to the low-density fractions after LubWX, but not TX-100, extraction.

In HepG2 cells, MDR1-GFP-association with LubWX-insoluble microdomains was further confirmed after in situ extraction with detergents. As shown in Figure 5C, b, after extraction with lubWX, MDR1-GFP remained associated with the BC surface, but was efficiently removed when cells had been extracted with 1% TX-100 (Figure 5C, c). These observations demonstrate in a direct manner that MDR1-GFP was associated with LubWX-insoluble microdomains at the AP surface of HepG2 cells.

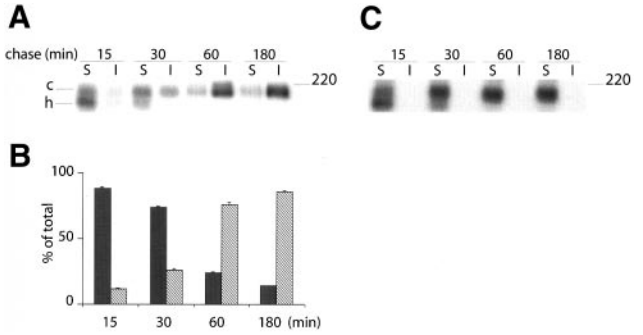

Figure 6. Kinetics of MDR1-GFP in LubWX-resistant domains revealed by pulse-chase analysis. MDR1-GFP–expressing cells were ^{35}S-labeled for 10 min, followed by incubation in chase medium for the indicated times. Cells were extracted either in TNE/LubWX buffer (A) or in TNE/TX-100 buffer (C) at 4°C, and processed as in Figure 2C. In B, quantification of three independent experiments, after extraction with LubWX, is shown as mean ± SD. Black bars represent soluble protein and hatched bars represent insoluble protein.

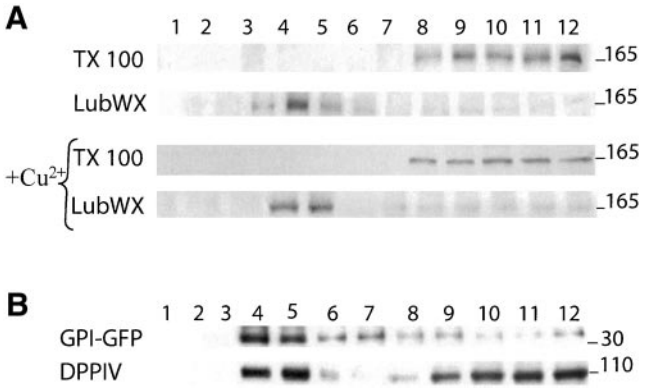

Figure 7. ATP7B is soluble in TX-100 but insoluble in LubWX. (A) Endogenous ATP7B, present in HepG2 cells, was analyzed for lipid microdomain association on sucrose density gradients after lysis of the cells either in TNE/TX-100 or TNE/LubWX at 4°C, in the absence of copper or after treatment for 4 h with 20 μM $CuSO_4$ ($+Cu^{2+}$). (B) Flotation of GPI-GFP and DPPIV in sucrose gradients after extraction with LubWX.

To further define where MDR1-GFP became associated with LubWX-insoluble microdomains, MDR1-GFP-expressing cells were ^{35}S-pulse–labeled for 10 min and then chased for 15–180 min. As shown in Figure 6, A and B, after a 15-min chase, MDR1-GFP was almost entirely soluble, a major fraction was present as the high mannose precursor but evidently, also the mature form was still largely LubWX soluble. After 30 min of chase, the fraction of MDR1 present as matured complex, increased. Concomitantly, the LubWX-insoluble fraction also increased and rapidly gained in size over the next 30 min. After 180 min, >90% of ^{35}S-labeled MDR1-GFP had become integrated into LubWX-insoluble microdomains. These results indicate that the LubWX insolubility of MDR1-GFP is acquired during biosynthetic transport. Interestingly, also in these experiments, ^{35}S-labeled MDR1-GFP could not be detected in TX-100–insoluble fractions at any time (Figure 6C), thus also excluding its potential transient association with TX-100 microdomains. Together, these observations raise the possibility that direct protein transport between TGN and BC in HepG2 cells, mediated by LubWX-insoluble microdomains, could rely on the multispanning membrane properties of MDR1. To examine this possibility further, we investigated the trafficking of another polytopic protein, ATP7B.

ATP7B Trafficking between Golgi and BC Is Mediated by LubWX-insoluble Microdomains

ATP7B is a copper-transporting P-type ATPase with eight putative TMD, and in response to copper, relocates from the TGN to the BC surface in HepG2 cells (Bull *et al.*, 1993; Tanzi *et al.*, 1993; Roelofsen *et al.*, 2000). Analogous to MDR1 (see above) and consistent with a direct transport pathway, no ATP7B could be detected at the BL membrane at steady state (our unpublished data). Moreover, after treatment with TX-100, ATP7B was recovered in the soluble fractions, whereas after treatment with LubWX, ATP7B was found to float to the low-density fractions (Figure 7A). These results demonstrate that like MDR1-GFP, ATP7B integrates into LubWX- and not in TX-100–insoluble microdomains. Note that at these conditions, i.e., without the addition of exogenous copper, the protein is largely, if not exclusively, localized in TGN (Roelofsen *et al.*, 2000). Yet, the same results were obtained when lipid microdomains were purified from HepG 2 cells cultured in the presence of exogenous copper (Figure 7A). This indicates that ATP7B already associated with LubWX-insoluble microdomains at the TGN and remained firmly associated with such domains, after arrival at the BC surface.

The exclusive preference of the investigated polytopic proteins to integrate into LubWX-insoluble microdomains for direct transport between TGN and BC, prompted a revisit of the findings for the indirect pathway, concerning the detergent specificity of lipid microdomains. As shown in Figure 7B, next to TX-100 resistance (Figure 2A), GPI-GFP and DPPIV were also resistant to LubWX extraction. Quantification revealed that whereas GPI-GFP was entirely insoluble in both detergents, a significant increase in the floating fraction of DPPIV was observed when extracting the cells with LubWX (from 15 to 34%). In conjunction with the distinct detergent-dependent sensitivity toward extraction in situ (Figure 2B) and the observed apparent differences in efficiency of BC-directed transport, these observations may well imply that DPPIV and GPI-GFP are at least in part localized at different BL domains.

To obtain further insight into the functional specificity of either DRM type, we took into account the role of cholesterol as a crucial parameter in DRM stability, and addressed the question whether perturbation of the cholesterol pool could distinctly affected the sorting and/or trafficking in either pathway.

Removal of Cholesterol Leads to an Alteration in the Insolubility of GPI-GFP and DPPIV

To examine the role of cholesterol in the sorting of GPI-GFP, GPI-GFP–expressing cells were treated with Lov/CD as

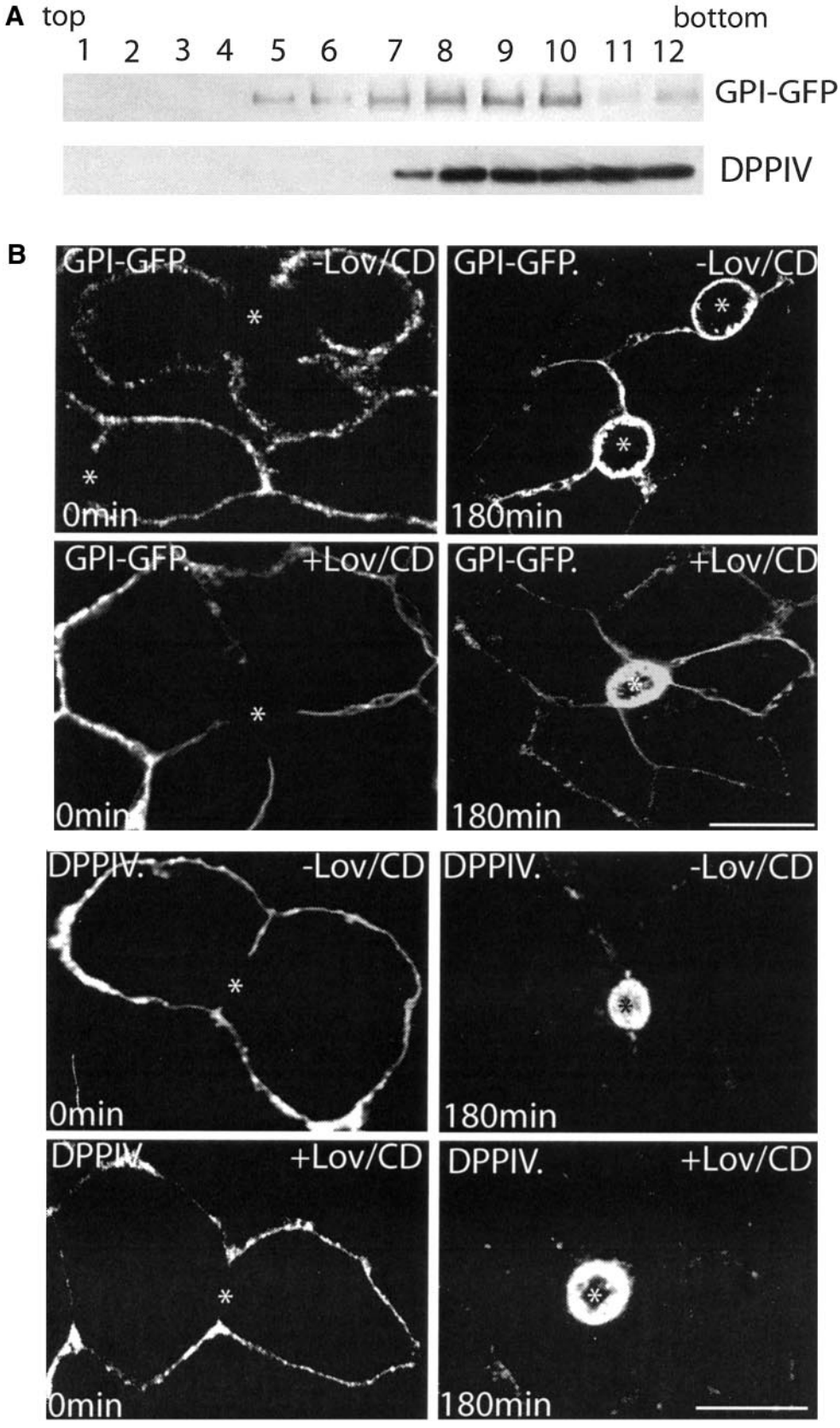

Figure 8. Cholesterol removal renders GPI-GFP and DPPIV less TX-100 insoluble without affecting their AP targeting. (A) GPI-GFP–expressing cells were grown in the presence of Lov/CD as described under MATERIALS AND METHODS. Cells were then lysed in TNE/TX-100 buffer and analyzed by flotation on sucrose gradient. (B) GPI-GFP–expressing cells were grown in the absence (−Lov/CD) or presence (+Lov/CD) of Lov/CD. The dynamics of GPI-GFP and DPPIV was investigated using the trafficking antibody assay as in Figure 1B. *, BC. Bar, 10 μm.

described under MATERIALS AND METHODS. HepG2 cells treated in this way lost ~50% of their cholesterol (our unpublished data). We found that relative to control cells (Figure 2A), cholesterol depletion caused a shift of GPI-GFP and DPPIV to the high density, i.e., soluble fractions upon gradient analysis of the TX-100 extracts (Figure 8A). Apparently, cholesterol depletion leads to a disruption of the interaction of GPI-GFP and DPPIV with lipid microdomains, traveling along the indirect pathway in HepG2 cells. However, as shown in Figure 8B, except for a potentially diminished transport efficiency, reflected by the larger fractions of GPI-GFP remaining associated with the BL membranes after cholesterol depletion, removal of cholesterol does not seem to significantly affect AP targeting of GPI-GFP and DPPIV.

Cholesterol Depletion Does Not Affect the LubWX Insolubility of MDR1-GFP but Leads to Its Partial Mistargeting to the Basolateral Surface

As shown in Figure 9A, in the direct pathway, cholesterol depletion did not affect the LubWX insolubility of MDR1-GFP, suggesting that cholesterol is not crucial for the association of MDR1-GFP with LubWX-insoluble microdomains. Importantly, we obtained direct evidence for the actual presence of cholesterol in both TX-100– and LubWX-insoluble microdomains (Figure 9B)

To verify the specificity of this observation, we also analyzed the effect of cholesterol depletion on the LubWX insolubility of GPI-GFP and DPPIV. Also in this case, major fractions of both GPI-GFP and DPPIV were shifted from the low- to the high-density fractions, although seemingly to a slightly lower extent than in the case of cholesterol-depleted TX-100 microdomains (Figure 9A vs. 8A). This distinction could also explain why DPPIV is seemingly more effectively transported in cholesterol-depleted cells than GPI-GFP, the latter showing a more exclusive dependence on TX-100–insoluble microdomains transport than DPPIV (Figure 8B), which shows a relative higher recovery in LubWX domains (Figure 2A vs. 7B).

We next investigated the effect of cholesterol depletion on the cell surface expression of MDR1-GFP by immunofluorescence. Surprisingly, although a considerable proportion of MDR1-GFP was still present at the BC surface, a significant amount of the protein now occurred on the BL membrane and in intracellular structures (Figure 9C). To rule out the possibility that the BL localization of MDR1-GFP was due to an artificial disruption of the tight junction, MDR1-GFP–expressing cells were incubated for 30 min at 0°C with BODIPY-SM to label the BL membrane. As revealed by confocal microscopy, whereas MDR1-GFP was localized at both the BC and the BL membrane, BODIPY-SM was exclusively restricted to the BL membrane (Figure 9D). These results indicate that HepG2 cells remained properly polarized after Lov/CD treatment, implying that cholesterol depletion caused a genuine MDR1-targeting defect.

The MDR1-GFP found at the BL membrane of cholesterol-depleted cells, could have originated either from the biosynthetic pathway or from the BC surface. To discriminate between these possibilities, MDR1-GFP–expressing cells were incubated for 60 min in the presence of 25 μg/ml cycloheximide to inhibit protein synthesis. Cells were then treated with Lov/CD for 60 min in the continued presence of cycloheximide. After such treatment, GFP fluorescence was no longer observed at the BL membrane (Figure 9E), indicating that the basolaterally localized MDR1-GFP in cholesterol-depleted cells originated from the biosynthetic pathway. Hence, these data suggest that cholesterol depletion did not affect AP membrane-directed trafficking, but rather caused mistargeting of newly synthesized MDR1.

To obtain further support for this notion, we next investigated whether correct targeting could be reestablished, after replenishment of cellular cholesterol by addition of CD/Chol complexes, as described previously (Zuhorn *et al.*, 2002). As can be seen in Figure 9, F and G, after restoring cholesterol levels, MDR1-GFP was no longer detected at the BL membrane, displaying again its prominent presence at the BC surface, thus indicating that cholesterol is crucial for the correct AP trafficking of MDR1.

DISCUSSION

The present study demonstrated that in polarized hepatic cells raft-mediated trafficking is involved in both the direct and indirect pathways, along which resident apical membrane proteins reach the bile canalicular membrane. Detergent specificity suggests that distinct, pathway-specific microdomains are operating. Whereas LubWX-insoluble, but TX-100–soluble microdomains traffic in the direct pathway, domains insoluble in both LubWX and TX-100 carry the investigated proteins in the indirect pathway. The data also hinted that sorting into either apical transport pathway in polarized HepG 2 cells may rely on the nature of the membrane-anchoring domain, polytopic proteins entering the direct and single TMD, or GPI-anchored proteins entering the indirect transcytotic pathway (Table 1). Most importantly, all apically targeted proteins examined herein, exploit a lipid microdomain-sorting principle, which implies that in liver cells, raft-mediated trafficking is not exclusively associated with direct apical targeting.

Resident Apical Proteins Are Recruited into Lipid Microdomains in the TGN for Both Direct and Indirect Transport

The raft hypothesis proposes that apical proteins are selectively incorporated into lipid microdomains in the TGN and are then transported directly to the apical membrane (Simons and Ikonen, 1997). In the majority of epithelial cells studied, such a mechanism has been shown for all GPI-anchored proteins (Lisanti *et al.*, 1988, 1989; Brown *et al.*, 1989; Soole *et al.*, 1995; Kenworthy and Edidin, 1998), and some TMD proteins (Kundu *et al.*, 1996; Huang *et al.*, 1997; Lin *et al.*, 1998). However, in hepatocytes, transcytotic delivery via the basolateral membrane has been proposed to represent the major pathway for delivery of resident apical proteins (Schell *et al.*, 1992; Maurice *et al.*, 1994; Ihrke *et al.*, 1998). Indeed, also in polarized HepG2 cells a GPI-anchored fusion protein uses the transcytotic pathway and, moreover, is recovered in TX-100– and LubWX-insoluble microdomains. Yet, membrane multispanning MDR1 and ATP7B never reached the BL membrane, traveling directly to the AP membrane in LubWX-insoluble microdomains. Of relevance, similarly to that previously described in other cell lines (Brown and Rose, 1992; Garcia *et al.*, 1993; Zurzolo *et al.*,

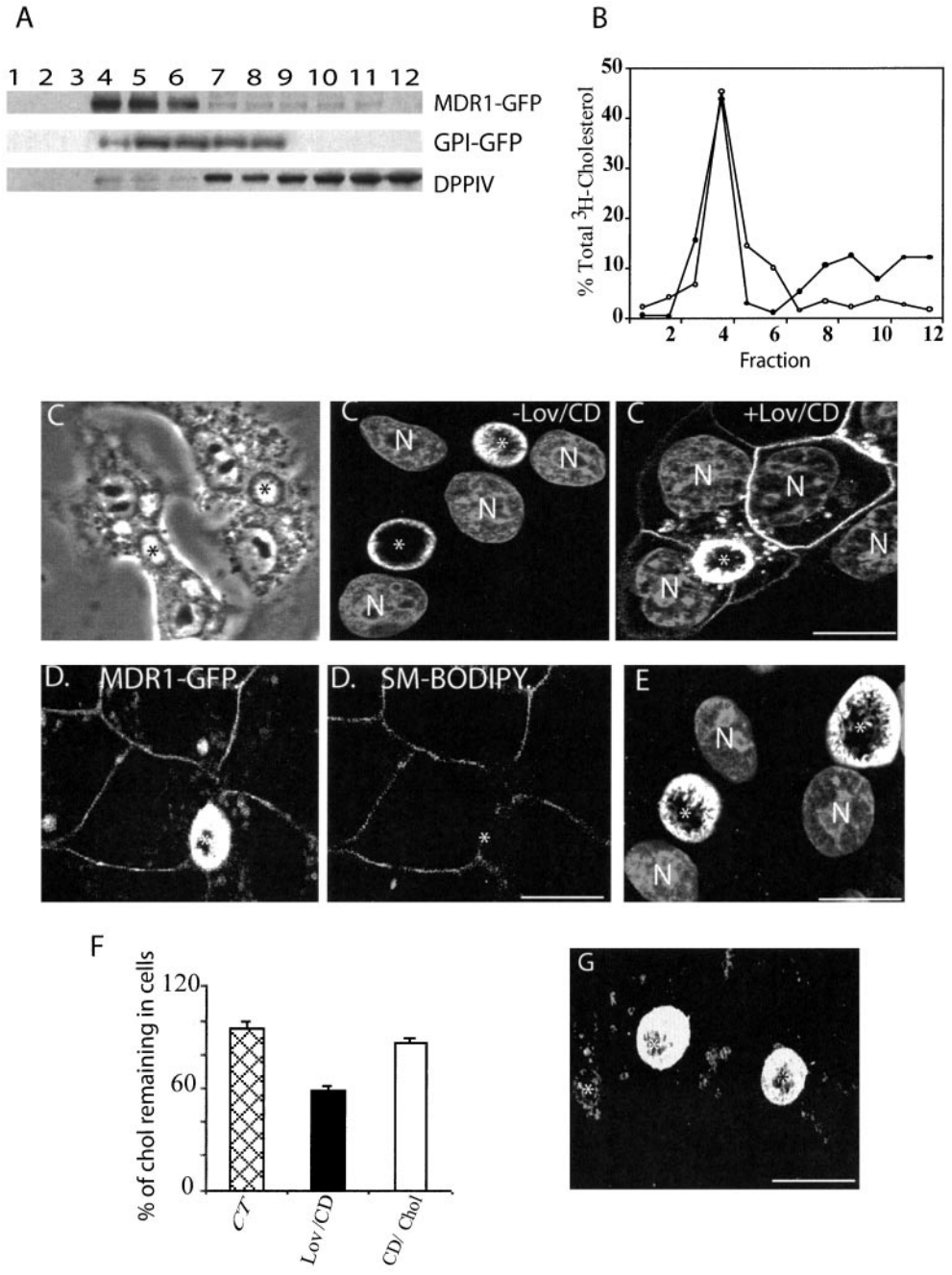

Figure 9. Cholesterol depletion causes missorting of MDR1-GFP without affecting its insolubility in LubWX. (A) MDR1-GFP– and GPI-GFP–transfected cells were treated as in Figure 8, and then lysed in TNE/LubWX buffer and processed as in Figure 8A. (B) HepG 2 cells were incubated with [^{3}H]cholesterol for 24 h at 37°C and subsequently washed and solubilized with either TX-100 or LubWX buffer. The lysates were then analyzed by sucrose gradient ultracentrifugation. Gradient fractions were collected from the top of the tube and [^{3}H]cholesterol was measured by liquid scintillation counting. The results indicate the percentage of total [^{3}H]cholesterol determined in each fraction. ○, LubWX; ●, TX-100. (C) MDR1-GFP–expressing cells were treated with (+Lov/CD) or without (−Lov/CD) Lov/CD, fixed, permeabilized, and examined by confocal microscopy. A phase contrast image of Lov/CD-treated cells is shown at the top, left. (D) MDR1-GFP–expressing cells treated with Lov/CD were incubated for 30 min at 0°C with SM-BODIPY and subsequently analyzed by confocal microscopy. (E) MDR1-GFP–expressing cells were incubated in the presence of cycloheximide for 60 min and subsequently treated with Lov/CD in the continuous presence of cycloheximide. After fixation and permeabilization, the cells were examined by confocal microscopy. Nuclei (N) are stained with propidium iodide. (F) The cholesterol concentration of control, cholesterol-depleted, and cholesterol-repleted cells was determined (see MATERIALS AND METHODS for details). Data were obtained from three independent experiments. (G) Cholesterol-depleted cells were grown in the presence of CD/Chol complexes as described under MATERIALS AND METHODS and subsequently examined for the localization of MDR1-GFP. *, BC. Bar, 10 μm.

Table 1. Summary of the properties of the trafficking pathways in polarized HepG 2 cells

			DRM		Cholesterol depletion	
Protein	Structure	Pathway	TX 100	LubWX	Insolubility	Localization
GPI-GFP	GPI anchored	Indirect	Insoluble	Insoluble	Affected	Not affected
DPPIV	Single TMD	Indirect	Insoluble	Insoluble	Affected	Not affected
APN	Single TMD	Indirect	ND		ND	
MDR1	Multispanning	Direct	Soluble	Insoluble	Not affected	Missorted
ATP7B	Multispanning	Direct	Soluble	Insoluble	ND	

ND, not determined.

1993), the kinetics by which all proteins investigated herein acquire detergent resistance indicates that also in liver cells, recruitment into lipid microdomains occurs in the biosynthetic pathway at the level of the Golgi (Figures 3A and 6A). Also, a low-temperature–trafficking block precludes Golgi exit (Figure 2E). Hence, in both pathways the Golgi acts as an important intracellular site for DRM assembly. Accordingly, direct apical sorting cannot be solely driven by incorporation into rafts per se.

As revealed by in situ extractions (Figure 2B), once reaching the basolateral membrane, raft-based mechanisms are also operational in delivery of GPI-linked apical resident proteins along the transcytotic pathway, presumably via subapical compartment (SAC) (Ihrke *et al.*, 1998), where distinct sphingolipid domains have been identified (van IJzendoorn and Hoekstra, 1999b). Although the presence of rafts in the SAC of HepG2 cells remains to be determined, evidence has been provided that recycling endosomes in MDCK cells (Gagescu *et al.*, 2000), as well as the common endosome in enterocytes (Hansen *et al.*, 1999), both bearing reminiscence to the SAC, contain raft components.

Distinctions in Lubrol Raft-mediated Trafficking in Direct and Indirect Pathway

The direct pathway is characterized by LubWX-insoluble microdomain-mediated trafficking of the multispanning MDR1-GFP in both HepG2 and MDCK cells (Figure 5), suggesting that the same direct apical sorting machinery for MDR1 may be operating in both cell lines. LubWX-insoluble microdomains also harbor the multispanning membrane proteins prominin and synaptophysin and the ABC transporter ABCA1 (Roper *et al.*, 2000; Drobnik *et al.*, 2002), and as shown herein, also the polytopic PM protein ATP7B. Furthermore, the LubWX-insoluble microdomains in direct and indirect pathway differ, not only because of their obvious difference in cargo protein content but also because only LubWX-insoluble microdomains in the indirect, transcytotic pathway are TX-100 insoluble. The same was noted for the GPI-anchored placental alkaline phosphatase in MDCK cells and for two other GPI-anchored proteins, CD14 and CD55 in human monocytes, which are also recovered in both LubWX- and TX-100–insoluble microdomains (Roper *et al.*, 2000; Drobnik *et al.*, 2002). Moreover, in the indirect pathway, LubWX microdomains localized GPI-GFP becomes more soluble after cholesterol depletion without affecting its apical targeting, whereas at the same conditions the LubWX insolubility of MDR1-GFP is not affected. Accordingly, these data may suggest a structural diversity of both LubWX-resistant domains, which may rely, for example, on differences in lipid ordering that would affect detergent accessibility and hence, detergent solubility (Madore *et al.*, 1999). Indeed, one could readily envision that a relatively less ordered raft domain could more easily accommodate the helical domains of multispanning membrane proteins. Triton solubility of the LubWX rafts in the direct pathway, but not in the indirect pathway, would be consistent with this notion. In this context, our preliminary data, comparing the lipid composition of TX-100– and LubWX-insoluble microdomains, revealed that LubWX microdomains were enriched in distinct phospholipids, whereas both domains contain a very similar glycosphingolipid composition (our unpublished data).

Role of Cholesterol in Apical Sorting in Polarized Hepatic Cells

Lowering cholesterol levels, e.g., by cyclodextrin treatment, leads to the disruption of rafts (Keller and Simons, 1998; Ilangumaran and Hoessli, 1998, Hansen *et al.*, 2000). In polarized MDCK cells, cholesterol depletion increases the solubility of HA and diverts its transport from predominantly apical to basolateral (Keller and Simons, 1998), although enhanced solubility has also been claimed not to correlate with its mistargeting (Lin *et al.*, 1998). In FRT cells, Lipardi *et al.* (2000) have shown that removal of cholesterol does not affect apical sorting of two GPI-anchored proteins, although it increases their solubility in TX-100. Also, as recently reported, cholesterol may not be crucial for raft assembly, and rafts may exist as stable cholesterol-independent microdomains (Hansen *et al.*, 2001; Milhiet *et al.*, 2002). Our data indicate that in HepG2 cells cholesterol is required for the association of GPI-GFP with lipid microdomains. In contrast, removal of cholesterol does not affect the insolubility of MDR1-GFP in LubWX. The distinctive response to cholesterol removal may reflect differences in interacting lipids and/or proteins in the different DRM and/or implicate a prominent role of either protein's membrane domain in raft association. Most interestingly, as a functional consequence of cholesterol depletion, seemingly little if any effect was observed on the indirect apical sorting of GPI-GFP and DPPIV, whereas mislocalization of newly synthesized MDR1-GFP to the basolateral surface occurred. Hence, cholesterol is crucial for the correct transport of MDR1-GFP to

the BC surface. It is tempting to speculate that a cholesterol-dependent sorting factor, becoming activated in the biosynthetic pathway, causes missorting. This suggestion follows from the notion that in polarized HepG2 cells, rafts per se, being active in both pathways, are not sufficient as sorting principle as such. Hence, the present study should pave the way for revealing novel molecular mechanisms underlying structural and functional properties of raft-mediating sorting and trafficking in polarized cells in general and in hepatic cells in particular.

ACKNOWLEDGMENTS

We thank Andre Le Bivic and Irwin M. Arias for the generous gift of cDNAs; Ann. L Hubbard, Hans-Peter Hauri, Jean-Louis Delaunay, and Han Roelofsen for providing antibodies; and Michele Maurice (Institut National de la Santé et de la Recherche Médicale U538, Paris, France) and the members of the Hoekstra laboratory, in particular Joke van der Wouden, for stimulating discussions.

REFERENCES

Bartles, J.R., Feracci, H.M., Stieger, B., and Hubbard, A.L. (1987). Biogenesis of the rat hepatocyte plasma membrane in vivo: comparison of the pathways taken by apical and basolateral proteins using subcellular fractionation. J. Cell Biol. *105*, 1241–1251.

Bastaki, M., Braiterman, L.T., Johns, D.C., Chen, Y.H., and Hubbard, A.L. (2002). Absence of direct delivery for single transmembrane apical proteins or their "secretory" forms in polarized hepatic cells. Mol. Biol. Cell *13*, 225–237.

Brown, D.A., Crise, B., and Rose, J.K. (1989). Mechanism of membrane anchoring affects polarized expression of two proteins in MDCK cells. Science *245*, 1499–1501.

Brown, D.A., and Rose, J.K. (1992). Sorting of GPI-anchored proteins to glycolipid-enriched membrane subdomains during transport to the apical cell surface. Cell *68*, 533–544.

Bull, P.C., Thomas, G.R., Rommens, J.M., Forbes, J.R., and Cox, D.W. (1993). The Wilson disease gene is a putative copper transporting P-type ATPase similar to the Menkes gene. Nat. Genet. *5*, 327–337.

Casanova, J.E., Mishumi, Y., Ikehara, Y., Hubbard, A.L., and Mostov, K.E. (1991). Direct apical sorting of rat liver dipeptidylpeptidase IV expressed in Madin-Darby canine kidney cells. J. Biol. Chem. *266*, 24428–24432.

Drobnik, W.,. Borsukova, H., Bottcher, A., Pfeiffer, A., Liebisch, G., Schutz, G.J., Schindler, H., and Schmitz, G. (2002). Apo AI/ABCA1-dependent and HDL3-mediated lipid efflux from compositionally distinct cholesterol-based microdomains. Traffic *4*, 268–278.

Gagescu, R., Demaurex, N., Parton, R.G., Hunziker, W., Huber, L.A., and Gruenberg, J. (2000). The recycling endosome of Madin-Darby canine kidney cells is a mildly acidic compartment rich in raft components. Mol. Biol. Cell *11*, 2775–2791.

Gamble, W., Vaughan, M., Kruth, H.S., and Avigan, J. (1978). Procedure for determination of free and total cholesterol in micro- or nanogram amounts suitable for studies with cultured cells. J. Lipid Res. *19*, 1068–1070.

Garcia, M., Mirre, C., Quaroni, A., Reggio, H., and Le Bivic, A. (1993). GPI-anchored proteins associate to form microdomains during their intracellular transport in Caco-2 cells. J. Cell Sci. *104*, 1281–1290.

Gribar, J.J., Ramachandra, M., Hrycyna, C.A., Dey, S., and Ambudkar, S.V. (2000). Functional characterization of glycosylation-deficient human P-glycoprotein using a vaccinia virus expression system. J. Membr. Biol. *173*, 203–214.

Hansen, G.H., Niels-Christiansen, L.L., Immerdal, L., Hunziker, W., Kenny, A.J., and Danielsen, E.M. (1999). Transcytosis of immunoglobulin A in the mouse enterocyte occurs through glycolipid raft- and rab17-containing compartments. Gastroenterology *3*, 610–622.

Hansen, G.H., Immerdal, L., Thorsen, E., Niels-Christiansen, L.L., Nystrom, B.T., Demant, E.J., and Danielsen, E.M. (2001). Lipid rafts exist as stable cholesterol-independent microdomains in the brush border membrane of enterocytes. J. Biol. Chem. *276*, 32338–32344.

Hansen, G.H., Niels-Christiansen, L.L., Thorsen, E., Immerdal, L., and Danielsen, E.M. (2000). Cholesterol depletion of enterocytes. Effect on the Golgi complex and apical membrane trafficking. J. Biol. Chem. *275*, 5136–5142.

Hemery, I., Durand-Schneider, A.M., Feldmann, G., Vaerman, J.P., and Maurice, M. (1996). The transcytotic pathway of an apical plasma membrane protein (B10) in hepatocytes is similar to that of IgA. and occurs via a tubular pericentriolar compartment. J. Cell Sci. *109*, 1215–1227.

Huang, X.F., Compans, R.W., Chen, S., Lamb, R.A., and Arvan, P. (1997). Polarized apical targetting directed by the signal/anchor region of simian virus 5 hemagglutinin-neuraminidase. J. Biol. Chem. *272*, 27598–27604.

Ihrke, G., Martin, G.V., Shanks, M.R., Schrader, M., Schroer, T.A., and Hubbard, A.L. (1998). Apical plasma membrane proteins and endolyn-78 travel through a subapical compartment in polarized WIF-B hepatocytes. J. Cell Biol. *141*, 115–133.

Ikonen, E. (2001). Roles of lipid rafts in membrane transport. Curr. Opin. Cell Biol. *13*, 470–477.

Ilangumaran, S., and Hoessli, D.C. (1998). Effects of cholesterol depletion by cyclodextrin on the sphingolipid microdomains of the plasma membrane. Biochem J. *335*, 433–440.

Keller, P., and Simons, K. (1998). Cholesterol is required for surface transport of influenza virus hemagglutinin. J. Cell Biol. *140*, 1357–1367.

Kenworthy, A.K., and Edidin, M. (1998). Distribution of a glycosylphosphatidylinositol-anchored protein at the apical surface of MDCK cells examined at a resolution of <100 A using imaging fluorescence resonance energy transfer. J. Cell Biol. *142*, 69–84.

Kipp, H., and Arias, I.M. (2000). Newly synthesized canalicular ABC transporters are directly targeted from the Golgi to the hepatocyte apical domain in rat liver. J. Biol. Chem. *275*, 15917–15925.

Kundu, A., Avalos, R.T., Sanderson, C.M., and Nayak, D.P. (1996). Transmembrane domain of influenza virus neuraminidase, a type II protein, possesses an apical sorting signal in polarized MDCK cells. J. Virol. *70*, 6508–6515.

Le Bivic, A., Quaroni, A., Nichols, B., and Rodriguez-Boulan, E. (1990). Biogenetic pathways of plasma membrane proteins in Caco-2, a human intestinal epithelial cell line. J. Cell Biol. *111*, 1351–1361.

Lin, S., Naim, H.Y., Rodriguez, A.C., and Roth, M.G. (1998). Mutations in the middle of the transmembrane domain reverse the polarity of transport of the influenza virus hemagglutinin in MDCK epithelial cells. J. Cell Biol. *142*, 51–57.

Lipardi, C., Nitsch, L., and Zurzolo, C. (2000). Detergent-insoluble GPI-anchored proteins are apically sorted in Fischer rat thyroid cells, but interference with cholesterol or sphingolipids differentially affects detergent insolubility, and apical sorting. Mol. Biol. Cell *11*, 531–542.

Lisanti, M.P., Caras, I.W., Davitz, M.A., and Rodriguez-Boulan, E. (1989). A glycophospholipid membrane anchor acts as an apical targeting signal in polarized epithelial cells. J. Cell Biol. *109*, 2145–2156.

Lisanti, M.P., Le Bivic, A., Saltiel, A.R., and Rodriguez-Boulan, E. (1990). Preferred apical distribution of glycosyl-phosphatidylinositol (GPI) anchored proteins: a highly conserved feature of the polarized epithelial cell phenotype. J. Membr. Biol. *113*, 155–167.

Lisanti, M.P., Sargiacomo, M., Graeve, L., Saltiel, A.R., and Rodriguez-Boulan, E. (1988). Polarized apical distribution of glycosyl-phosphatidylinositol-anchored proteins in a renal epithelial cell line. Proc. Natl. Acad. Sci. USA *85*, 9557–9561.

Low, S.H., Wong, S.H., Tang, B.L., Subramaniam, V.N., and Hong, W.J. (1991). Apical cell surface expression of rat dipeptidyl peptidase IV in transfected Madin-Darby canine kidney cells. J. Biol. Chem. *266*, 13391–13396.

Madore, N., Smith, K.L., Graham, C.H., Jen, A., Brady, K., Hall, S., and Morris, R. (1999). Functionally different GPI proteins are organized in different domains on the neuronal surface. EMBO J. *24*, 6917–6926.

Maier, O., Ait Slimane, T., and Hoekstra, D. (2001). Membrane domains and polarized trafficking of sphingolipids. Semin. Cell Dev. Biol. *12*, 149–161.

Matter, K., Brauchbar, M., Bucher, K., and Hauri, H.P. (1990). Sorting of endogenous plasma membrane proteins occurs from two sites in cultured human intestinal epithelial cells (Caco-2). Cell *60*, 429–437.

Matter, K., and Mellman, I. (1994). Mechanisms of cell polarity: sorting and transport in epithelial cells. Curr. Opin. Cell Biol. *6*, 545–554.

Maurice, M., Schell, M.J., Lardeux, B., and Hubbard, A.L. (1994). Biosynthesis and intracellular transport of a bile canalicular plasma membrane protein: studies in vivo and in the perfused rat liver. Hepatology *19*, 648–655.

Milhiet, P.E., Giocondi, M.C., and Le Grimellec, C. (2002). Cholesterol is not crucial for the existence of microdomains in kidney brush-border membrane models. J. Biol. Chem. *277*, 875–878.

Mostov, K.E., Verges, M., and Altschuler, Y. (2000). Membrane traffic in polarized epithelial cells. Curr. Opin. Cell Biol. *12*, 483–490.

Nelson, W.J., and Yeaman, C. (2001). Protein trafficking in the exocytic pathway of polarized epithelial cells. Trends Cell Biol. *11*, 483–486.

Nichols, B.J., Kenworthy, A.K., Polishchuk, R.S., Lodge, R., Roberts, T.H., Hirschberg, K., Phair, R.D., and Lippincott-Schwartz, J. (2001). Rapid cycling of lipid raft markers between the cell surface and Golgi complex. J. Cell Biol. *153*, 529–541.

Rodriguez-Boulan, E., and Powell, S.K. (1992). Polarity of epithelial and neuronal cells. Annu. Rev. Cell Biol. *8*, 395–427.

Roelofsen, H., Wolters, H., Van Luyn, M.J., Miura, N., Kuipers, F., and Vonk, R.J. (2000). Copper-induced apical trafficking of ATP7B in polarized hepatoma cells provides a mechanism for biliary copper excretion. Gastroenterology *119*, 782–793.

Roper, K., Corbeil, D., and Huttner, W.B. (2000). Retention of prominin in microvilli reveals distinct cholesterol-based lipid microdomains in the apical plasma membrane. Nat. Cell Biol. *2*, 582–592.

Sai, Y., Nies, A.T., and Arias, I.M. (1999). Bile acid secretion and direct targeting of mdr1-green fluorescent protein from Golgi to the canalicular membrane in polarized WIF-B cells. J. Cell Sci. *112*, 4535–4545.

Schell, M.J., Maurice, M., Stieger, B., and Hubbard, A.L. (1992). 5′nucleotidase is sorted to the apical domain of hepatocytes via an indirect route. J. Cell Biol. *119*, 1173–1182.

Simons, K., and Ikonen, E. (1997). Functional rafts in cell membranes. Nature. *387*, 569–572.

Soole, K.L., Jepson, M.A., Hazlewood, G.P., Gilbert, H.J., and Hirst, B.H. (1995). Epithelial sorting of a glycosylphosphatidylinositol-anchored bacterial protein expressed in polarized renal MDCK and intestinal Caco-2 cells. J. Cell Sci. *108*, 369–377.

Tanzi, R.E., Petrukhin, K., Chernov, I., Pellequer, J.L., Wasco, W., Ross, B., Romano, D.M., Parano, E., Pavone, L., and Brzustowicz, L.M. (1993). The Wilson disease gene is a copper transporting ATPase with homology to the Menkes disease gene. Nat. Genet. *5*, 344–350.

van der Woude, I., A. Wagenaar, A.A. Meekel, M.B. ter Beest, M.H. Ruiters, J.B. Engberts, and Hoekstra, D. (1997). Novel pyridinium surfactants for efficient, nontoxic in vitro gene delivery. Proc. Natl. Acad. Sci. USA *94*, 1160–1165.

van IJzendoorn, S.C., and Hoekstra, D. (1999a). The subapical compartment: a novel sorting center?. Trends Cell Biol. *9*, 144–149.

van IJzendoorn, S.C., and Hoekstra, D. (1999b). Polarized sphingolipid transport from the subapical compartment: evidence for distinct sphingolipid domains. Mol. Biol. Cell *10*, 3449–3461.

Zacharias, D.A., Violin, J.D., Newton, A.C., and Tsien, R.Y. (2002). Partitioning of lipid-modified monomeric GFPs into membrane microdomains of live cells. Science *3*, 913–916.

Zegers, M.M.P., and Hoekstra, D. (1997). Sphingolipid transport to the apical plasma membrane domain in human hepatoma cells is controlled by PKC and PKA activity: a correlation with cell polarity in HepG2 cells. J. Cell Biol. *138*, 307–321.

Zuhorn, I.S., Kalicharan, R., and Hoekstra, D. (2002). Lipoplex-mediated transfection of mammalian cells occurs through the cholesterol-dependent clathrin-mediated pathway of endocytosis. J. Biol. Chem. *17*, 18021–18028.

Zurzolo, C., Le Bivic, A., Quaroni, A., Nitsch, L., and Rodriguez-Boulan, E. (1992). Modulation of transcytotic and direct targeting pathways in a polarized thyroid cell line. EMBO J. *11*, 2337–2344.

Zurzolo, C., Lisanti, M.P., Caras, IW., Nitsch, L., and Rodriguez-Boulan, E. (1993). Glycosylphosphatidylinositol-anchored proteins are preferentially targeted to the basolateral surface in Fischer rat thyroid epithelial cells. J. Cell Biol. *121*, 1031–1039.